Modeling of Reoxidation Inclusion Formation During Filling of Steel Castings

Kent D. Carlson and Christoph Beckermann

Department of Mechanical and Industrial Engineering,
The University of Iowa, Iowa City, IA 52242, USA

Keywords: Reoxidation inclusion, steel casting, simulation, inclusion modeling

Abstract

A reoxidation inclusion model is described that simulates the entire life cycle of inclusions during the filling of steel castings and predicts their final location in the casting. Inclusions can be released into the mold at the inlet and/or nucleate on the metal free surface, where contact with oxygen from the atmosphere creates them. Inclusion motion is calculated by solving an equation of motion for each inclusion at each time step. The growth of reoxidation inclusions is modeled both by oxide growth due to oxygen pickup at the liquid metal free surface as well as by inclusion agglomeration (combination) when inclusions come close enough together to merge. All of these pieces of the inclusion model have been implemented in commercial casting simulation software, and an application is provided to qualitatively compare the simulation results to experimental results. Also, a series of simulations are performed to examine the effect of various parameters specified in the model.

Introduction

The removal of oxide inclusions from steel castings and the subsequent repair of those castings are expensive and time consuming procedures. Svoboda et al. [1] estimated that twenty percent of the cost of producing steel castings is due to the removal of inclusions and the repair of the resulting defect areas with weld metal. Inclusions that remain in the casting adversely affect machining and mechanical performance, and may cause the casting to be rejected for failing to meet the radiographic standard requirements specified by the customer regarding allowable inclusion severity.

Reoxidation inclusions, which form when deoxidized steel comes into contact with oxygen during mold filling, make up a substantial portion of the inclusions found in steel castings. Griffin and Bates [2] estimated that 83% of the macro-inclusions found in low-alloy steel castings are reoxidation inclusions, as are 48% of those found in high-alloy steel castings. A typical reoxidation inclusion is depicted in Figure 1a. As seen in this figure, inclusions are often globular in appearance, and composed of several different oxides. The globular appearance seen in Figure 1a indicates that at least one of the oxides is in liquid form during formation, later solidifying to form the shape seen in this figure. In fact, reoxidation in low-alloy steels can also generate gaseous oxides, namely carbon monoxide (CO). However, if CO forms during filling, it quickly escapes from the surface into the atmosphere, rather than remaining in the casting to form a defect. The primary source of oxygen in reoxidation inclusion formation is believed to be the atmosphere, which contacts the metal stream during pouring and the metal free surface in the mold cavity during filling (see Figure 1b). The growth of inclusions is determined by the

oxidation rate, which is controlled by oxygen transport in the atmosphere [3]. The oxidation rate is thus a function of the partial pressure of oxygen in the atmosphere, the free surface area, local flow conditions, and thermophysical properties.

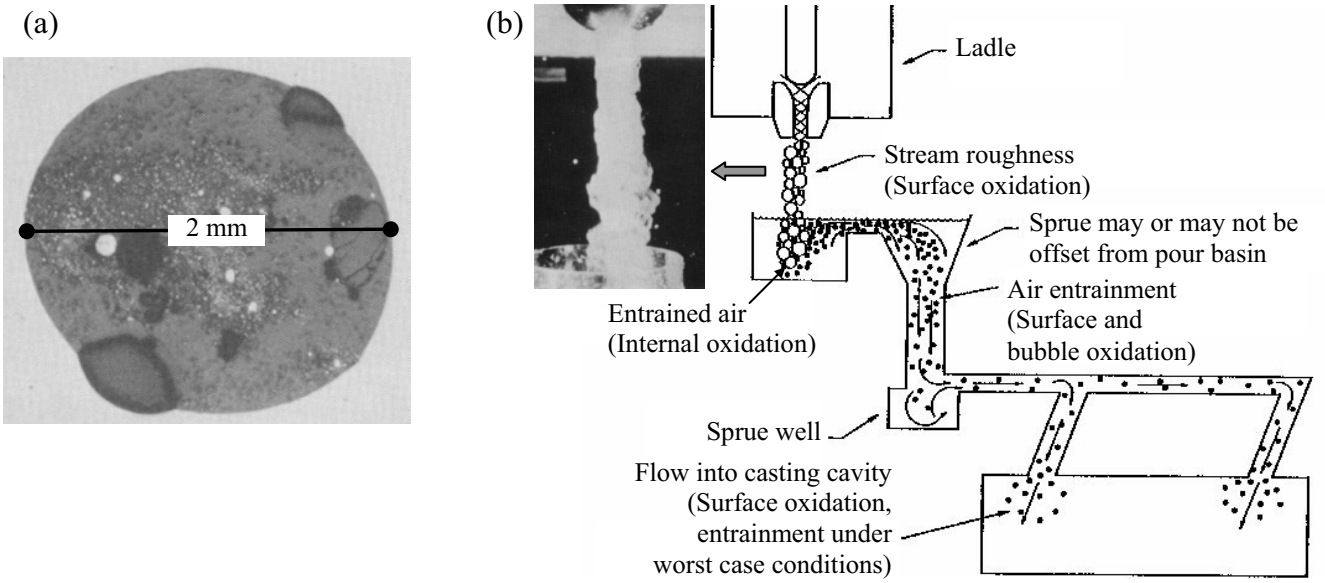

Figure 1: (a) Optical micrograph of a reoxidation inclusion cut from a test plate casting. The bulk composition is 34 wt% Al_2O_3, 46 wt% SiO_2, and 20 wt% MnO [2]; (b) Opportunities for oxygen absorption during mold filling (figure adapted from [2]).

At present, trial-and-error and experience are the only tools that foundry engineers have at their disposal to solve inclusion problems in steel castings. If a casting has inclusion problems, the foundry engineer may change the pouring practice or gating design for the casting in hopes that this will eliminate or reduce the severity of the problem. Changing the pouring or gating will change melt flow patterns during filling. This may reduce the amount of reoxidation inclusions created, or it may merely change the final location of macro-inclusions; if the inclusions are swept into a riser rather than collecting on the cope surface of the casting, the inclusion problem may be solved even if the volume of reoxidation inclusions created does not change. In order to avoid inclusion problems or to reduce their severity, foundries often employ special filling techniques to reduce the contact area and time between the melt and the atmosphere during mold filling or to trap inclusions inside the runners. Thus, several iterations on the rigging of a casting may be necessary to resolve inclusion issues.

In an attempt to provide foundry engineers with a tool for eliminating or minimizing inclusion problems, a model is being developed that simulates the formation, growth, and motion of reoxidation inclusions during the pouring of steel castings. This model, which is being developed within commercial casting simulation software [4], will allow foundries to predict the final location, size, number and other characteristics of reoxidation inclusions in a casting. The various components of the inclusion model that are currently implemented in the simulation software are described in the next section. The modeling section is followed by a presentation of a preliminary application of this model to perform a parametric study and to compare simulation results with experimental results. It is stressed that the present model is still being refined and that the results in this paper are still preliminary.

Modeling Inclusion Formation, Growth, Agglomeration, and Motion

This section describes the different aspects of the current inclusion model. These aspects include inclusion formation, growth, agglomeration and motion. In the modeling discussion that follows, all inclusions are assumed to be spheres characterized by a diameter *d*, with a constant density ρ_{incl}.

Formation

The present model provides two mechanisms that can be used to create reoxidation inclusions: release and birth (nucleation). These mechanisms can be used separately or together. The release mechanism allows the user to release inclusions at the inlet to the mold. This option can be used to model tiny deoxidation or other larger inclusions that enter from the ladle into the casting cavity with the melt during pouring. This way, the effects of the cleanliness of the melt from the ladle can be examined. The user specifies the characteristics of the released inclusions by choosing an initial diameter, d_{rel} (cm) and inclusion number density, n_{rel} (cm^{-3}).

The birth mechanism creates tiny new inclusions on the free surface of the melt during filling. In the present model, the initial size of the inclusions that nucleate on the free surface is assumed to be negligibly small. In practice, a small but finite value is used for the initial diameter, such that the initial inclusion volume is still negligibly small. The user specifies a "nucleation" spacing, l_0 (cm), which indicates the desired initial spacing between inclusions that nucleate on the free surface. Note that the nucleation spacing is related to the number of nuclei per unit free surface area, n_0'' (cm^{-2}), by the relation $n_0'' = l_0^{-2}$. An important point to consider when specifying the nucleation spacing is that using a very small nucleation spacing (~10 microns) comparable to experimentally observed values [5] would result in a total number of inclusions that is too large for present-day computing resources. Hence, a compromise must be found that provides final results that are reasonably independent of the number of inclusions generated by the birth model and that can be obtained within present computational capabilities. This issue is examined in detail in the section concerning application of the model.

The model determines whether or not birth occurs in each computational cell containing a free surface by determining the average spacing, l_{exist} (cm), between existing inclusions in that cell. If the spacing between existing inclusions exceeds the user-specified nucleation spacing, l_0, then inclusion birth occurs in the available free surface area in the cell. If no inclusions are present in a free surface cell, the existing spacing is set to a large distance, which ensures that the nucleation spacing is exceeded and that inclusion birth occurs in the cell. It is necessary to have at least one inclusion in every free surface cell in order to accurately predict the total volume of inclusions formed. The number of inclusions that nucleate, N_{birth}, is determined from

$$N_{birth} = n_0'' A_{birth} = l_0^{-2} A_{birth} \tag{1}$$

where A_{birth} (cm^2) is the free surface area available in the cell, which is the cell free surface area minus the free surface area taken up by existing inclusions in the cell. This number is then rounded up to the nearest integer, and N_{birth} inclusions are added to the free surface cell, spaced a distance of l_0 apart.

Growth

When inclusions are on the melt free surface, they will absorb oxygen from the atmosphere and grow as a result. The rate of inclusion growth is controlled by oxygen transport in the atmosphere, as noted earlier [3]. Note that inclusions within the melt (i.e., not on the free surface) will not grow, because there is a negligible amount of dissolved oxygen in liquid steel. Assuming a constant inclusion density, the inclusion growth is modeled by the equation

$$dV_{incl}/dt = A_{FS,incl}\beta \tag{2}$$

In this equation, V_{incl} is the inclusion volume (cm^3); $A_{FS,incl}$ is the area (cm^2) of the melt free surface that is contributing oxide to the growing inclusion; and β is an effective, overall mass transfer coefficient (cm/s). The model currently assumes that β is a constant; however, a model enhancement under development treats this coefficient as a variable that accounts for variations in the oxidation rate due to changes in the flow conditions, the partial pressure of oxygen in the atmosphere, etc.

In the present growth model, the total oxidation rate is proportional to the entire free surface area at any instant of time. However, the amount of oxide formed during a given time step must be apportioned to the individual inclusions. This can be done in a cell-by-cell manner, since each free surface cell has at least one inclusion (due to the birth model described above). The present apportioning procedure is based on the idea that larger inclusions "attract" oxide from a larger portion of the free surface than do smaller inclusions. Hence, in order to determine the area $A_{FS,incl}$ in Equation (2), it is assumed that the total flow cell free surface area, $A_{FS,cell}$ (cm^2), is divided among the inclusions within that flow cell, proportional to each inclusion's current surface area.

Equation (2) is solved for the volume of each inclusion after growth, V_{incl}, and then the corresponding inclusion diameter is given by

$$d = \left(6V_{incl}/\pi\right)^{1/3} \tag{3}$$

Agglomeration

Aside from growth, inclusions can also increase in size during filling by colliding and merging with each other, to form a single larger inclusion. This is known as agglomeration. While this can happen anywhere in the melt due to random collisions, it is more likely to occur on the liquid metal free surface. This is because solid inclusions on the liquid free surface cause small indentations in the free surface. These indentations extend beyond the inclusions themselves, and essentially create an attractive force over very small distances (on the order of ten to a few hundred microns). The size of the indentation made by each inclusion is a function of the liquid metal surface tension and the size and density of the inclusion. In the present agglomeration model, if two inclusions are within some critical distance L_{crit} of each other, they are assumed to agglomerate immediately. The assumption of instantaneous agglomeration neglects the inertia and drag forces on the particles during agglomeration; it is necessary because of the difficulty in resolving the motion of the inclusions over the small distances involved in the agglomeration process.

To determine if two inclusions agglomerate, it is necessary to determine the critical distance L_{crit} (cm). This was done using the experimental data of Shibata et al. [6]. They measured accelerations and separation distances of agglomerating inclusions on a horizontal free surface in low-carbon aluminum-killed (LCAK) steel, in order to determine the attractive forces and critical distances between inclusions. They found that the critical distance depends primarily on the radius of the larger of the two inclusions. Using the data of Shibata et al. [6], the following relationship was developed between the radius of the larger inclusion and the critical distance:

$$L_{crit}\ (\text{cm}) = 0.084\sqrt{d_{\max}/2} \tag{4}$$

where $d_{\max}$ (cm) is the diameter of the larger of the two inclusions. It is important that the diameter used in Equation (4) is in centimeters, because the constant in front of the square root has units of ($\text{cm}^{1/2}$). As an example, if the larger inclusion has a diameter of 5 mm (= 0.5 cm), the critical distance is 0.042 cm (= 420 microns). Note that Equation (4) is an approximate relationship that was determined from data for a horizontal free surface in LCAK steel. This relationship is very approximate for different alloys (due to differences in surface tension) and different surface orientations. However, it does provide the necessary mechanism for short-distance inclusion attraction on free surfaces. Also note that the critical distance given in Equation (4) is only valid if both inclusions involved are on the metal free surface. If one or both are immersed in the metal, the attractive surface force is absent, and a critical distance of $L_{crit} = 0$ is used. Finally, note that more than two inclusions can be involved in an agglomeration. If several inclusions on the free surface are close enough to a given inclusion to satisfy the agglomeration criterion, all inclusions within this distance are combined.

When inclusions agglomerate, it is necessary to determine the properties of the newly formed inclusion. This is done by first summing the volumes of the inclusions involved, to determine the volume of the agglomerated group, V_{agg} (cm^3). The diameter of the new inclusion, d_{agg} (cm), is then determined from the equation relating the volume of a sphere to its diameter (as in Equation (3)). The position of the new inclusion is given by the center of mass of the inclusions that were involved in the agglomeration, and the velocity of the new inclusion is determined by conservation of linear momentum.

Motion

In order to determine the final location of inclusions, it is necessary to track their movement from the time they form until filling is complete. In the present model, this is done by solving the following equation of motion for each inclusion, at each time step:

$$m_{incl}\frac{d\vec{v}_{incl}}{dt} = F_{drag} + F_{buoyancy} \tag{5}$$

where m_{incl} and $\vec{v}_{incl}$ are the mass (kg) and velocity (cm/s) of the inclusion, respectively; and F_{drag} and $F_{buoyancy}$ are the drag and buoyancy forces (kg-cm/s^2) acting on the inclusion. Since agglomeration of inclusions is assumed to be instantaneous (see the previous sub-section), no attraction forces between inclusions are included in the above equation. Other forces (virtual mass, lift, drag due to the presence of other inclusions, etc.) are also neglected. In addition, Equation (5) assumes that the inclusion mass is constant during motion. Since inclusions are assumed to be spherical, Equation (5) can be expressed as

$$\rho_{incl}\frac{d\vec{v}_{incl}}{dt}=\frac{18\mu_l}{d_{incl}^2}\left(\vec{v}_l-\vec{v}_{incl}\right)\left(1+0.15\,\mathrm{Re}^{0.687}\right)+\left(\rho_{incl}-\rho_l\right)\vec{g} \tag{6}$$

where ρ_{incl} and d_{incl} are the density (kg/cm^3) and diameter (cm) of the inclusion, respectively; ρ_l and μ_l are the density (kg/cm^3) and dynamic viscosity (kg/cm-s) of the liquid metal, respectively; $\vec{g}$ is the gravity vector (cm/s^2); t is time (s); and Re is the Reynolds number, which is a dimensionless number defined in terms of the difference between the velocity of the inclusion ($\vec{v}_{incl}$) and the velocity of the surrounding liquid metal ($\vec{v}_l$) as

$$\mathrm{Re}=\frac{\left|\vec{v}_l-\vec{v}_{incl}\right|\rho_l d_{incl}}{\mu_l} \tag{7}$$

The first term on the right side of Equation (6) is the drag force, and the second term is the buoyancy force. The drag force is written in terms of a dimensionless drag coefficient, C_D, given by

$$C_D=\frac{24}{\mathrm{Re}}\left(1+0.15\,\mathrm{Re}^{0.687}\right) \tag{8}$$

This drag coefficient correlation is valid for $\mathrm{Re}\le 1000$.

During each time step of a filling simulation, Equation (6) is solved for each inclusion to determine its velocity. This information is then used to update the location of each inclusion according to $d\vec{x}_{incl}/dt=\vec{v}_{incl}$, where $\vec{x}_{incl}$ is the position vector of each inclusion. If an inclusion comes into contact with a mold wall, it is assumed to stick to the wall.

Application of the Model

This section describes the results of several simulations that were performed in order to evaluate the current state of the model. The geometry used in this study is the plate geometry shown in the upper left of Figure 2. The plate is 2.54 cm thick by 25.4 cm wide by 30.5 cm long (1 in. x 10 in. x 12 in.), with a 10.2 cm (4 in.) diameter by 10.2 cm (4 in.) high end riser. This particular geometry was selected because of the availability of experimental data with which to compare simulation results. Filling of this geometry is simulated for 1022 steel in a furan sand mold. The pouring temperature is 1581˚C (2878˚F), which gives a superheat of 80˚C (144˚F). The pouring time is 7 seconds.

The present investigation focuses on the birth model, so the inclusion release model is not employed in any of the simulations discussed here. As a first approximation, the inclusion density is taken to be equal to 0.003 kg/cm^3. The inclusion size at birth is specified as d_0 = 4 microns. This size is small enough that it results in an essentially negligible initial inclusion volume at birth. The mass transfer coefficient for these simulations is specified as β = 0.0002 cm/s; this value simply provides a reasonable growth rate for the purpose of the present simulations. As mentioned before, an improved oxidation rate model is currently under development.

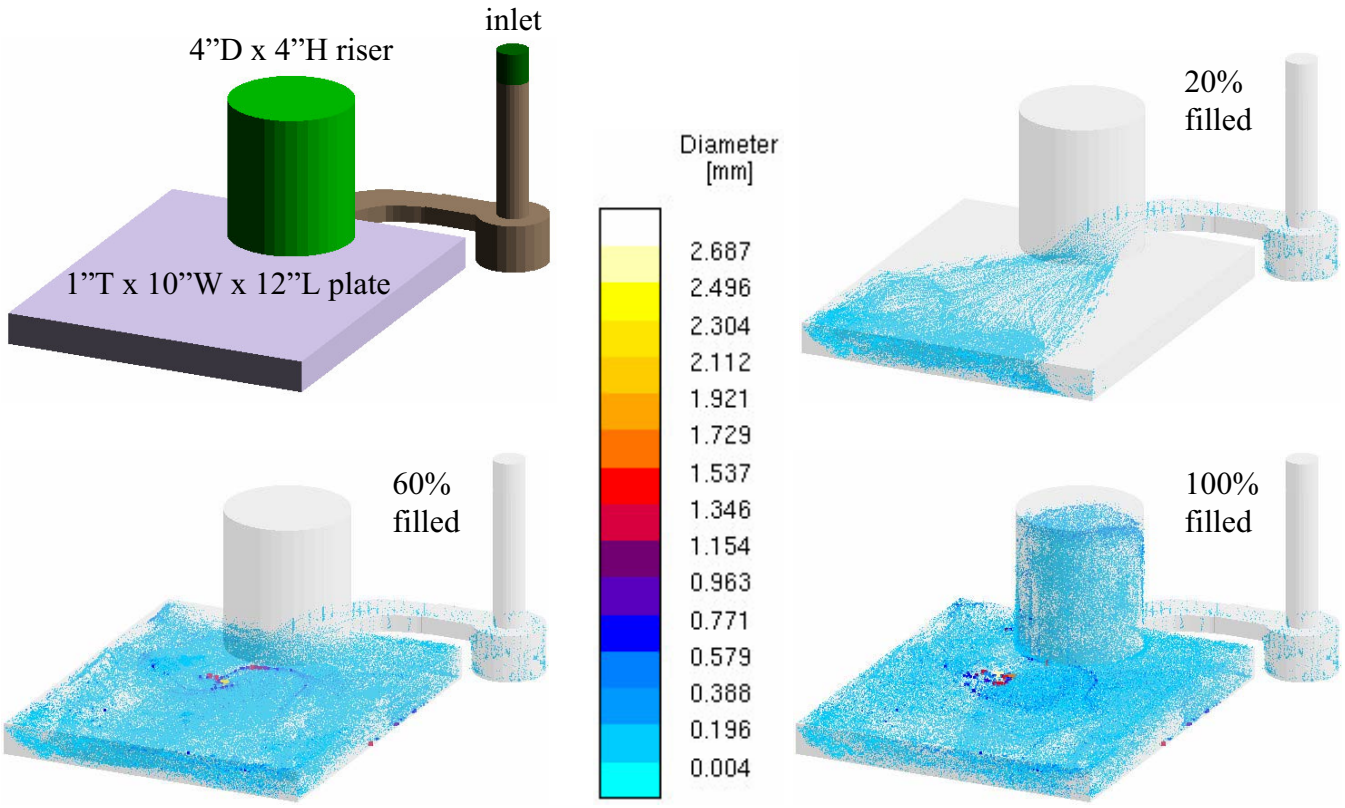

Figure 2: Simulated inclusions at various times during filling for Case 1. Inclusions shown at 3x magnification.

Other simulation parameters that must be specified include the grid size (or number of metal cells) and the nucleation spacing, l_0. These parameters were varied to produce the three cases listed in Table I.

Table I. Parameters and results for inclusion simulations.

Case	Inclusion spacing l_0 (cm) at birth	Number of metal cells	Number of inclusions generated	Final number of inclusions	Total inclusion volume (cm^3)	d_{max} (cm)	d_{avg} (cm)
1	0.5	26,053	212,604	146,522	0.276	0.269	0.0115
2	0.25	26,053	405,824	283,571	0.276	0.227	0.0091
3	0.25	13,263	302,876	219,285	0.279	0.210	0.0095

The simulated inclusions at several increments during filling are shown for Case 1 in Figure 2. As the plate becomes nearly filled (see “60% filled” in Figure 2), a group of relatively large inclusions are seen to form in the middle of the plate near the cope surface. This is caused by a swirling behavior of the liquid metal in this region when the plate is nearly filled. The swirling of the liquid metal brings many inclusions into the same area, where they agglomerate on the free surface to form the large inclusions seen on the plate cope surface in Figure 2 (“100% filled”). However, Figure 2 also shows that smaller inclusions (around 100 microns in diameter) are evenly distributed throughout the casting. A top view of the inclusions at the end of filling is shown in Figure 3a. This simulation result can be compared to the two experimental plates shown in Figure 3b. These plates were cast with the rigging shown in

Figure 2, and then 0.32 cm (⅛ in.) of material was machined from their cope surfaces. The circles drawn on the plates in Figure 3b are inclusion counts, where 2.54-cm (1-in.) diameter circles are drawn around all visible inclusions on the machined cope surfaces. Note that the locations of the inclusions seen in the experimental plates in Figure 3b are in good agreement with the locations of the largest inclusions shown in Figure 3a. The final inclusion plots produced for Cases 2 and 3 look qualitatively very similar to those of Case 1 in Figures 2 and 3a; therefore, they are not shown here. It is interesting to note, however, that even as the model parameters are varied, the simulated final locations of the largest inclusions match the experimental results.

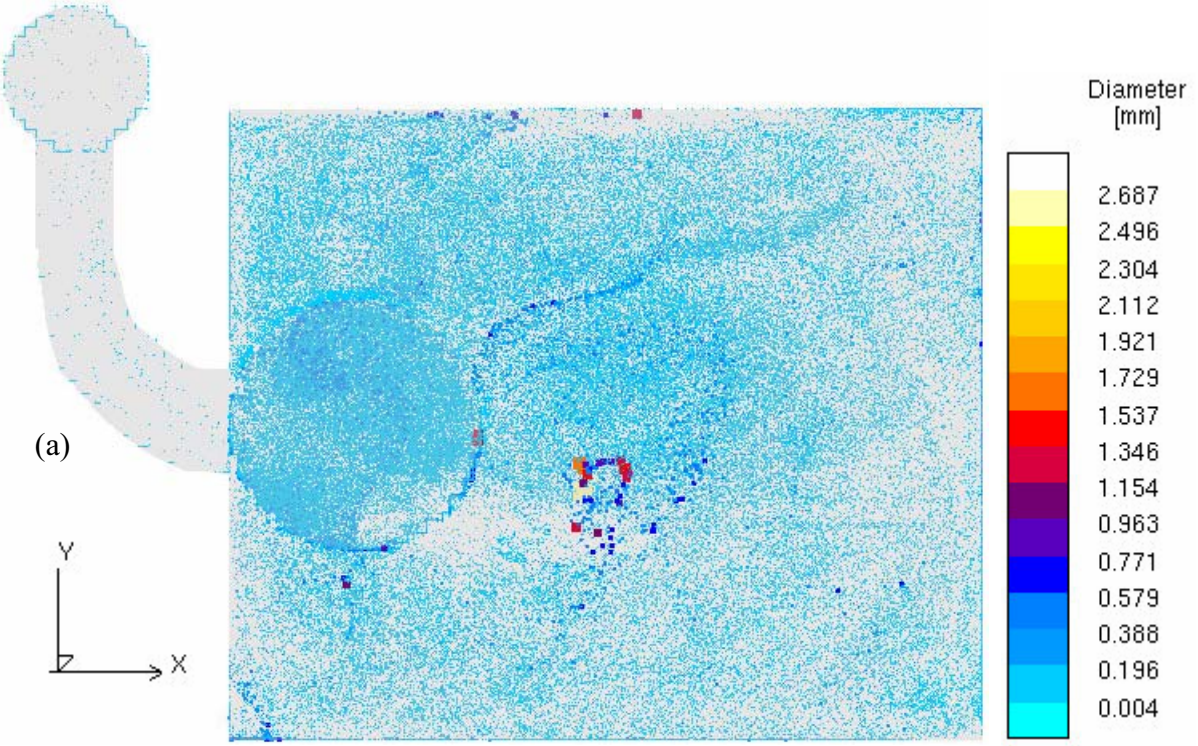

Figure 3: Comparison between simulation and experimental results: (a) Top view of final simulated inclusion locations. Inclusions shown at 3x magnification; (b) photo showing inclusion locations on the cope surface of two experimental plates.

Table I summarizes the results of the simulations of the three cases mentioned above. Furthermore, the final size and volume distributions of the inclusions for each case are presented in Figure 4. The plots on the left side of Figure 4 show the distribution of the number of inclusions for each case. Final inclusion diameter is plotted on the x-axis of these figures. The inclusions were grouped by their diameters into one-micron diameter increments and counted. This count (i.e., the number of inclusions in each one-micron interval) was then divided by the total number of inclusions at the end of the simulation and plotted on the y-axis, as the number fraction of inclusions per micron of diameter. Hence, the area under each of the curves on the left side of Figure 4 is equal to unity. These figures show the distribution of inclusions, based on their diameter. For example, Figure 4a shows that the majority of inclusions produced in this simulation have a final diameter of around 100 microns, with very few inclusions larger than 500 microns (0.5 mm). The plots on the right side of Figure 4 show the distribution of the final inclusion volume as a function of inclusion diameter. These figures also plot the final inclusion diameter on the x-axis, but now the total volume of the inclusions within each micron increment of diameter are computed and divided by the total volume of all inclusions. This is plotted on the y-axis, as the total final volume fraction per micron of diameter. The area under each of the curves on the right side of Figure 4 is also equal to unity. These figures relate the distribution of the total inclusion volume to the inclusion diameter. For example, Figure 4b shows that the majority of the final inclusion volume consists of inclusions 500 microns or smaller, with a peak around 200 microns. The presence of relatively few large inclusions can be clearly observed in the Figures 4b, 4d and 4f.

As shown in Table I, Case 1 used a grid with about 26,000 metal cells (i.e., cells that will contain metal at the end of filling) and a nucleation spacing of 0.5 cm. This simulation resulted in a final total inclusion volume of 0.276 cm^3, consisting of about 147,000 inclusions, with a maximum inclusion diameter of 0.269 cm (2.69 mm). A total of about 213,000 inclusions were generated, implying that about 66,000 inclusions combined together through agglomeration. Case 2 used all the same parameters as Case 1, except that the nucleation spacing was reduced from 0.5 cm to 0.25 cm. Table I shows that this smaller nucleation spacing in Case 2 resulted in a final count of about 284,000 inclusions, which is nearly twice as many inclusions as in Case 1. As in Case 1, Case 2 resulted in a final total inclusion volume of 0.276 cm^3. This shows that the total volume of oxide generated is not affected by the number of inclusions simulated. The average inclusion diameter is different for the two cases (Table I), since the same total inclusion volume is produced with a different number of inclusions. However, Table I shows that despite the vastly different number of inclusions generated in Cases 1 and 2, the final diameter of the largest inclusion is similar in both cases (2.7 and 2.3 mm, respectively). Comparing Figures 4a and 4c, it is seen that the normalized size distribution of the final inclusions is also very similar in both cases. The peaks in both figures are of the same magnitude and occur at diameters slightly under 100 microns. This indicates that the predicted final size distribution of the inclusions is not affected by the number of the inclusions simulated, if the size distribution is normalized by the total final number of inclusions. This result is important for trying to minimize the number of inclusions in a simulation in order to reduce computational times. The volume distributions for Cases 1 and 2 are also quite similar (Figures 4b and 4d). In particular, the presence of a few inclusions of a large volume is predicted in approximately the same manner in both cases. This implies that the prediction of the large inclusions is not strongly affected by the total number of inclusions simulated. Since the large inclusions are of primary concern to steel foundries, this finding again can be used to minimize the number of inclusions in a simulation. Although the curves are of a similar shape, note that the magnitude of the peak just below 200 microns is about 0.0038/micron in Figure 4b, while it is about 0.0048/micron in Figure 4d.

This indicates that more of the oxide volume is distributed among the smaller inclusions in Case 2 than in Case 1, which can be attributed to the larger total number of inclusions in Case 2 than in Case 1.

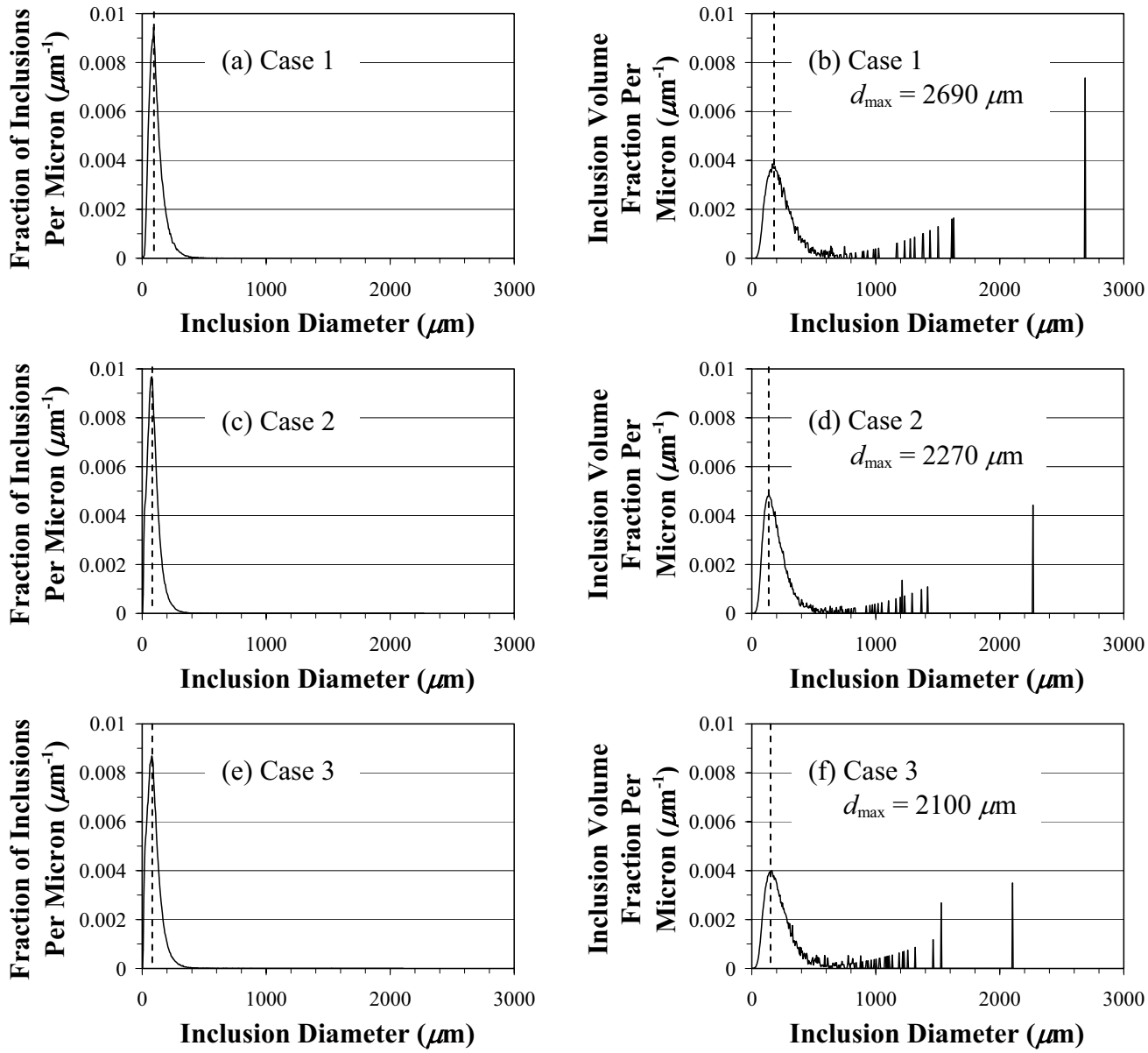

Figure 4: Distribution of number of inclusions based on diameter [(a), (c) and (e)] and inclusion volume based on diameter [(b), (d) and (f)] for Cases 1 – 3 shown in Table I.

Case 3 provides a check for grid independence: this case uses the same parameters as Case 2, except that it uses a grid that has about half the number of metal cells used in Case 2 (about 13,000). The total inclusion volume resulting for Case 3 is 0.279 cm^3, a value very close to the first two cases. Case 3 results in about 219,000 inclusions, which is a somewhat smaller number than in Case 2. However, both the maximum and average inclusion diameters in Case 3 are similar to Case 2. Comparing Figures 4c and 4e, it is seen that the normalized distribution of inclusions over the range of diameters is very similar. The peak value in Case 3 occurs at about the same diameter as in Case 2, although the fraction

of inclusions at the peak is about 10% smaller. Comparing Figures 4d and 4f, the trends are also very similar. Again, the peak volume fraction in Figure 4f is somewhat lower than in Figure 4d. This indicates that more of the volume in Case 3 comes from somewhat larger inclusions, which can be seen by comparing these figures in the range of about 700 to 1300 microns (0.7 – 1.3 mm). The similarity of the results from Cases 2 and 3 gives some confidence in the grid independence of the present inclusion formation model. It should be noted that the similarity between the results from Cases 2 and 3 also implies a degree of time step independence, because the time step was larger in Case 3 than in Case 2. The time step in the casting simulation software into which this model was incorporated is variable and automatically determined based on many factors, one of which is grid size. Coarser grids lead the software to use larger time steps.

An interesting overall observation from this study is that all the simulations discussed here produce about the same total volume of inclusions. Furthermore, the size and volume distributions in all three cases are similar when normalized with the total final number of inclusions. As mentioned when discussing Figures 2 and 3a, the inclusion simulation results at the end of filling for all three cases looked qualitatively very similar (i.e., the largest inclusions ended up in roughly the same location). It is encouraging to see similar results from the model as relatively arbitrary parameters, such as nucleation spacing and grid size, are varied.

Conclusions

As presented in this paper, the current inclusion model shows promising results. By comparing simulation results to visible cope surface reoxidation inclusions in corresponding experimental trials, good qualitative agreement was seen in the final location and size of inclusions. There are still enhancements to be made. The primary area of enhancement is to implement an improved oxidation rate model, such that the mass transfer coefficient, β, is a function of the local flow conditions. After further testing and validation, the refined model will provide foundries with a tool to understand and prevent troublesome reoxidation inclusions.

Acknowledgements

This work was prepared with the support of the U.S. Department of Energy (DOE) Award No. DE-FC36-02ID14225. However, any opinions, findings, conclusions, or recommendations expressed herein are those of the authors, and do not necessarily reflect the views of the DOE. We would like to thank Bob Bryant and Keokuk Steel Castings for carrying out the casting trials that produced the experimental inclusion results provided in this paper. We would also like to thank Malcolm Blair and Raymond Monroe of the SFSA for their helpful suggestions and guidance in this work.

References

1. J.M. Svoboda et al., “Appearance and Composition of Oxide Macroinclusions in Steel Castings,” *AFS Transactions*, 95 (1987), 187-202.

2. J.A Griffin and C.E. Bates, “Ladle Treating, Pouring and Gating for the Production of Clean Steel Castings” (Research Report No. 104, Steel Founders' Society of America, 1991).

3. K. Sasai and Y. Mizukami, “Effect of Stirring on Oxidation Rate of Molten Steel,” *ISIJ International*, 36 (1996), 388-394.

4. MAGMASOFT, MAGMA GmbH, Kackerstrasse 11, 52072 Aachen, Germany.

5, Y. Wang et al., “Reoxidation of Low-Carbon, Aluminum-Killed Steel,” *AIST Transactions (Iron & Steel Technology)*, February 2004, 87-96.

6. H. Shibata, H. Yin and T. Emi, “The Capillary Effect Promoting Collision and Agglomeration of Inclusion Particles at the Inert Gas-Steel Interface,” *Phil. Trans. R. Soc. Lond. A*, 356 (1998), 957-966.